Development of gas jet targets for laser-plasma experiments at near-critical density

J.L. Henares, P. Puyuelo-Valdes, F. Hannachi, T. Ceccotti, M. Ehret, F. Gobet, L. Lancia, J.-R. Marquès, J.J. Santos, M. Versteegen, et al.

Review of Scientific Instruments

RESEARCH ARTICLE | JUNE 21 2019

Development of gas jet targets for laser-plasma experiments at near-critical density

J. L. Henares ; P. Puyuelo-Valdes; F. Hannachi; T. Ceccotti; M. Ehret ; F. Gobet; L. Lancia ; J.-R. Marquès; J. J. Santos ; M. Versteegen ; M. Tarisien

Rev. Sci. Instrum. 90, 063302 (2019)
https://doi.org/10.1063/1.5093613

Review of Scientific Instruments ARTICLE scitation.org/journal/rsi

Development of gas jet targets for laser-plasma experiments at near-critical density

Cite as: Rev. Sci. Instrum. 90, 063302 (2019); doi: 10.1063/1.5093613
Submitted: 22 February 2019 • Accepted: 29 May 2019 •
Published Online: 21 June 2019

J. L. Henares,[1,a)] P. Puyuelo-Valdes,[1,2] F. Hannachi,[1] T. Ceccotti,[3] M. Ehret,[4,5] F. Gobet,[1] L. Lancia,[6] J.-R. Marquès,[6] J. J. Santos,[4] M. Versteegen,[1] and M. Tarisien[1]

AFFILIATIONS

[1]Centre d'Etudes Nucléaires de Bordeaux Gradignan, Université de Bordeaux, CNRS-IN2P3, Route du Solarium, 33175 Gradignan, France
[2]INRS-EMT, 1650 Blvd. Lionel-Boulet, Varennes, Quebec QC J3X 1P7, Canada
[3]LIDYL, CEA, CNRS, Université Paris-Saclay, CEA Saclay, 91191 Gif-sur-Yvette, France
[4]Université de Bordeaux, CNRS, CEA, CELIA (Centre Lasers Intenses et Applications) UMR 5107, 33400 Talence, France
[5]Institut für Kernphysik, Technische Universität Darmstadt, 64289 Darmstadt, Germany
[6]LULI, Ecole Polytechnique-CNRS-CEA-Université Paris VI, F-91128 Palaiseau, France

[a)]**Electronic mail:** henares@cenbg.in2p3.fr

ABSTRACT

Computational fluid dynamics simulations are performed to design gas nozzles, associated with a 1000 bars backing pressure system, capable of generating supersonic gas jet targets with densities close to the critical density for 1053 nm laser radiation (10^{21} cm^{-3}). Such targets should be suitable for laser-driven ion acceleration at a high repetition rate. The simulation results are compared to the density profiles measured by interferometry, and characterization of the gas jet dynamics is performed using strioscopy. Proton beams with maximum energies up to 2 MeV have been produced from diatomic hydrogen gas jet targets in a first experiment.

I. INTRODUCTION

Novel laser-based ion acceleration methods are under development due to the interest of ion production for a large field of applications (nuclear physics, protontherapy, astrophysics, pharmacology, etc.).[1,2] Up to now, laser-driven proton acceleration has mainly been performed focusing a high intensity laser on a solid target. For most common laser intensities (about 10^{19} W/cm^2), the leading acceleration mechanism is Target Normal Sheath Acceleration (TNSA).[3,4] It is nowadays quite a well-known mechanism and related targets are easy to produce and set up. However, the energy distribution of the accelerated ions is continuous over a wide energy range and the accompanying generation of debris and contaminants is a major problem at a high repetition rate. Gas jet targets represent a promising alternative due to the advantage of negligible debris and fast regeneration.[5] Electron acceleration up to 200 MeV has been demonstrated using gas targets produced with millimetric supersonic nozzles.[6,7] Recently, capillary nozzles[8] and shock nozzles[9] have been developed for high repetition rate operation. Laser-driven ion acceleration has been first studied with CO_2 lasers ($\lambda = 10\ \mu$m) with the production of "quasi-monoenergetic" beams.[10–12] The development of submillimetric supersonic nozzles and an increase in the backing pressure up to 400 bars has allowed us to study He^+ acceleration with Ti:Sa laser systems ($\lambda = 800$ nm), generating up to 250 keV in the laser transverse direction.[13,14] Recently, hydrogen gas jet targets have been used with an intense $\lambda = 1054$ nm laser system producing few hundreds of kilo-electron-volts in the laser longitudinal direction.[15] The aim of the computational fluid dynamics (CFD) simulations described in this article is to design a nozzle capable of producing gas jet targets suitable for laser-driven ion acceleration at $\lambda = 1053$ nm laser facilities[16,17] (i.e., with densities of the order of the laser critical density). In relativistic conditions, the critical density n_c of free electrons in plasma is defined as

$$n_c = \varepsilon_o \gamma m_e \frac{\omega_o^2}{e^2}, \quad (1)$$

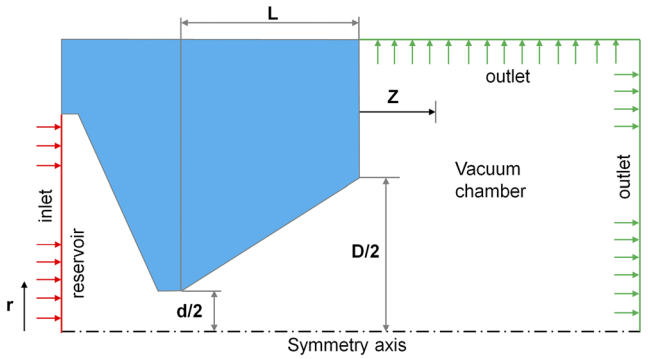

FIG. 1. Scheme of the 2D axisymmetric nozzle geometry used in CFD simulations (see text for details).

where ε_o is the vacuum permittivity, γ the relativistic factor, m_e the electron rest mass, ω_o is the angular frequency of the laser, and e is the electron charge.

Several ion acceleration mechanisms are predicted to compete during laser interaction with a near-critical density target [TNSA, hole boring, Collisionless Shockwave Acceleration (CSA), etc.] and only a proper optimization of the interaction parameters (target density, front and rear target plasma scale lengths, laser pulse characteristics, etc.) may allow one of them to lead the acceleration process.[18] Among them, CSA is probably the most promising mechanism since it is predicted to accelerate ions up to hundreds of megaelectronvolt in narrow energy bunches.[19]

II. FLUID DYNAMICS SIMULATIONS

CFD simulations are performed using the commercial software ANSYS FLUENT,[20] which numerically solves the Navier-Stokes equations on a discrete grid. An implicit density-based coupled solver (DBCS) is used with double precision accuracy green-Gauss node-based gradients of solution variables, to solve the stationary fluid flow. The standard k-omega model is used to model the turbulence. We have employed a 2D axisymmetric grid with quadrilateral cells, which typically consists of 2×10^5 cells with 2×10^{-2} average skewness ratio and minimum orthogonal quality of 8.5×10^{-1}. The grid is adapted to the surfaces, and we have verified that further refinements do not change the result of the simulation. A convergent-divergent supersonic conical nozzle is chosen for its ease of fabrication and its well known flow properties.[21] The nozzle is composed of a reservoir, a convergent section, a throat, and an expansion section giving to a chamber under vacuum. The geometrical parameters of the simulation are the throat diameter d, the nozzle exit diameter D, and the cone length L. The simulation also takes into account a wall roughness of 1 μm that micrometric nozzles machined by electro-erosion usually show. The boundary conditions of the simulation are a high-pressure at the inlet and two low pressures at the outlets in the vacuum chamber outside the nozzle. The distance from the nozzle exit is represented by Z (Fig. 1). The influence of the nozzle parameters on the gas jet properties has been studied in a previous study.[22] The inlet conditions are constant laminar flux and a free expansion of the gas in the vacuum (steady solution). The medium is diatomic hydrogen or diatomic nitrogen assumed to follow the real gas Peng-Robinson description with corresponding specific heat, thermal conductivity, and viscosity which depend on the pressure (see Table I). We have observed that the real gas Peng-Robinson equation better describes the behavior of the fluid than an ideal gas or other models in our range of pressures. The temperature of the inlet is 300 K, and the walls are supposed adiabatic. The maximum value of inlet pressure is limited by technical constraints to 1000 bars (1×10^8 Pa). The outlet pressures are set at 10^{-2} mbar (1 Pa) to reproduce the experimental conditions. The size of the vacuum chamber is chosen such as the gas can freely propagate, avoiding dilute flows. The net imbalance of mass and energy between the inlet and the outlet is verified to be less than 1% of the smallest flux through the domain boundary for flux conservation. An optimization of the geometrical parameters d, D, and L was carried out. The goal was to achieve a maximum of density at distances between 200 and 300 μm downstream by the formation of a Mach wave interference. A conical nozzle is selected with d = 100 μm, D = 200 μm, and L = 1 mm. This nozzle produces a parabolic density profile with a molecular density up to 1.6×10^{21} cm^{-3} of diatomic hydrogen (it is assumed that all the electrons of hydrogen atoms are

TABLE I. Heat capacity, thermal conductivity, and viscosity for hydrogen and nitrogen gas at 300 K at different inlet pressures from Refs. 23 and 24.

	Hydrogen				
	1 bar	50 bars	100 bars	500 bars	1000 bars
Heat capacity (J kg^{-1} K^{-1})	14 306	14 434	14 544	14 961	15 082
Thermal conductivity (W m^{-1} K^{-1})	1.85×10^{-1}	1.89×10^{-1}	1.93×10^{-1}	2.28×10^{-1}	3.19×10^{-1}
Viscosity (kg m^{-1} s^{-1})	8.915×10^{-6}	9.032×10^{-6}	9.153×10^{-6}	1.043×10^{-5}	1.236×10^{-5}
	Nitrogen				
	1 bar	50 bars	100 bars	500 bars	1000 bars
Heat capacity (J kg^{-1} K^{-1})	1 041.07	1 120.89	1 195.78	1 373.11	1 357.08
Thermal conductivity (W m^{-1} K^{-1})	2.61×10^{-2}	2.86×10^{-2}	3.13×10^{-2}	5.75×10^{-2}	8.67×10^{-2}
Viscosity (kg m^{-1} s^{-1})	1.79×10^{-5}	1.87×10^{-5}	2.00×10^{-5}	3.43×10^{-5}	5.35×10^{-5}

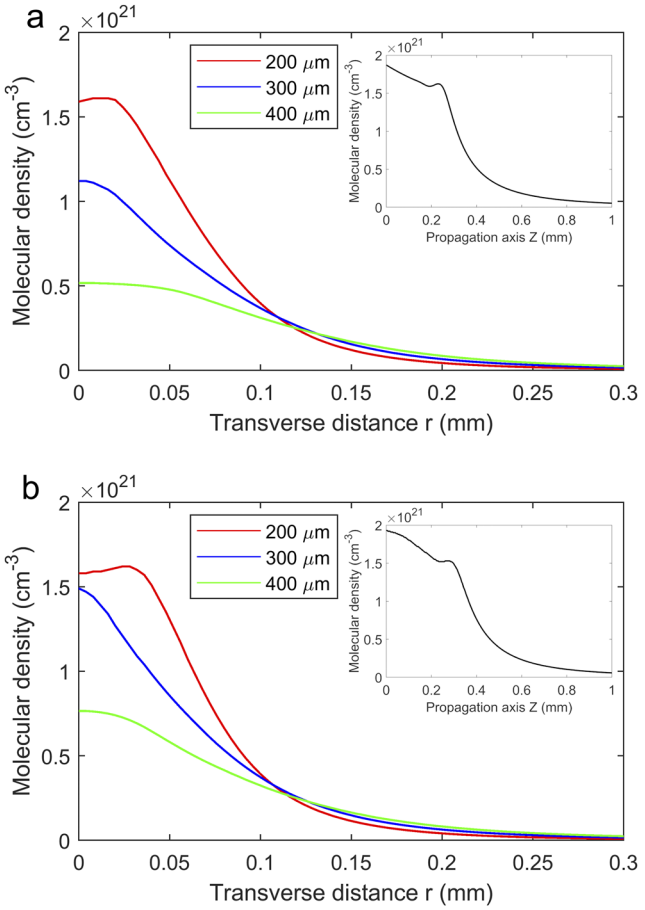

FIG. 2. Simulated molecular density profiles with (a) diatomic hydrogen and (b) diatomic nitrogen gas jets at a pressure of 1000 bars at Z = 200, 300, and 400 μm from the exit of the nozzle. The density gradient scale lengths at FWHM are 50 μm (Z = 200 μm), 74 μm (Z = 300 μm), and 85 μm (Z = 400 μm). The downstream propagation of the flow from the nozzle exit is shown in the inset figure. The increase of density due to the interference of Mach waves is observed.

ionized by the laser pulse, therefore the free electron density is twice the molecular density), with less than 150 μm FWHM at a distance of the nozzle exit ranging from Z = 200 to 400 μm (see Fig. 2).

III. GAS JET EXPERIMENTAL CHARACTERIZATION

In order to validate the CFD simulations, we have measured the real density profile delivered by the gas jet with a Mach-Zehnder interferometer using different gases [Fig. 3(a)]. The light radiation source we have employed is a ~20 mW Melles-Griot HeNe (632.8 nm) laser. A Kepler beam expander is installed to increase the beam diameter in order to cover all gas jet volume. A pinhole is placed in the expander focus, which spatially filters the laser beam, in order to remove noise from modes other than the Gaussian one and to obtain a homogeneous beam. The laser beam is divided by a beam splitter (BS) into reference and probe rays, with the probe ray passing through the gas jet. The two laser beams are recombined by another beam splitter to obtain a phase shift image. A half-wave plate is also installed to control the relative intensity of polarized light that goes to each arm of the interferometer. The gas jet nozzle is mounted on a Clark-Cooper solenoid valve EX30 that can provide continuous or pulsed gas flux. The high density is reached by using 1000 bars inlet pressure delivered by a Haskel gas booster model AGT-62/152. A lens images the phase shift interferogram onto a linear CCD camera PixelFly whose magnification allows us to get approximately 3 μm/pixel. The background noise of the interferometric image is reduced by subtracting the reconstructed image without gas (unperturbed condition). A good shot-to-shot stability and reproducibility is observed.

The phase shift induced by the gas flow is obtained by the fringe displacement from the unperturbed position in vacuum. A phase shift measurement allows the reconstruction of the gas jet density profile by means of variation of the refractive index n. Assuming a cylindrical symmetry of the gas jet (which is the case with axisymmetric nozzles) it is possible to reconstruct the density profile along one direction from a single phase shift image. The radial distribution of the refraction index is deduced using the Abel inversion. A description of the mathematical extraction of the phase shift variation and the Abel inversion can be found in Ref. 25. The phase shift calculation and the reconstruction of the density profile from the refractive index variation are performed by the analysis program Neutrino.[26] The gas molecule number density N is calculated from the general form of the Lorentz-Lorenz equation,[27]

$$N = \frac{3}{4\pi\alpha}\frac{n^2-1}{n^2+2}, \tag{2}$$

where α, the mean polarizability of the gas molecule, is defined as

$$\alpha = \frac{3A}{4\pi N_A}, \tag{3}$$

where A is the molar refractivity and N_A is Avogadro's number. Equation (3) can be combined with Eq. (2) to obtain

$$N = \frac{N_A}{A}\frac{n^2-1}{n^2+2}. \tag{4}$$

The molar refractivities for hydrogen and nitrogen are calculated from Eq. (4) (Table II) using refractive indices of gases from Ref. 28. It is known that they remain constant even at high pressures when n differs from unity.[27] An experimental measurement of nitrogen molar refractivity is described in Ref. 29 giving a value of 4.445 × 10^{-6} m^3/mol. We have used this value to reconstruct the density profiles shown in Fig. 4. Due to the opacity of the gas jet at high densities, reconstruction of the density is only possible in a moderate density region (10^{19}–10^{20} cm^{-3}). For this reason, the measurements are performed away from the exit of the nozzle (Z > 750 μm).

The density profiles obtained by interferometry are compared to the ones obtained by CFD simulations with diatomic nitrogen at 100 and 1000 bars and diatomic hydrogen at 100 bars (Fig. 4). The fluctuations in the central region of the profiles are artifacts due to the inherent noise of the Abel inversion close to the axis of symmetry and the imprecision of the symmetry axis position. The overall good agreement validates our simulations and gives us confidence in their results at 1000 bars with diatomic hydrogen.

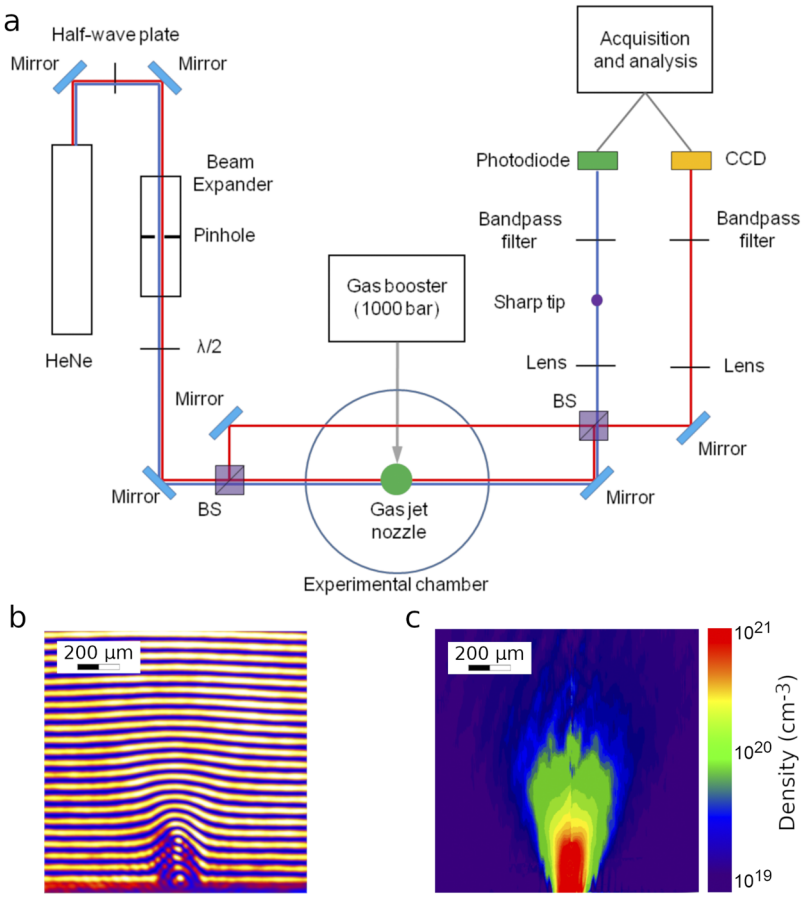

FIG. 3. (a) Scheme of the Mach-Zehnder interferometer (red line). Strioscopy (blue line) is set up by blocking the reference ray in the interferometer and by including a sharp object in the focus of the imaging lens (Fourier's plane). The signal is detected by a photodiode. (b) Interferogram obtained with N_2 at 1000 bars backing pressure and (c) density reconstruction considering an axisymmetric nozzle.

IV. DYNAMICS OF THE GAS JET

During the experiment, a solenoid valve is used to produce pulsed gas jets. A perfect characterization of the dynamics of the gas flux is mandatory to trigger the laser interaction when the maximum density of the gas jet is reached. The evolution of the gas flow is measured by strioscopy (based on the Schlieren effect). Strioscopy is an optical Fourier process in which the light diffused from an object is filtered by an obstacle blocking the Gauss mode and the diffracted light is measured [Fig. 3(a)]. The refractive index gradient of the object deflects the light in different optical path lengths, and the turbulences generated by the density gradient can be detected.[30] This method allows us to find the precise moment of flow stabilization and its duration for different gases, pressures, and opening time durations of the solenoid valve.

TABLE II. Calculated values of molar refractivity of hydrogen and nitrogen (using refractive index values from Ref. 28).

Hydrogen (m^3/mol)	2.094×10^{-6}
Nitrogen (m^3/mol)	4.506×10^{-6}

In Fig. 5, one can see the gas flow evolution for different opening time durations. The rising time of the gas jet corresponds to the time needed to completely fill the nozzle reservoir volume (about 230 mm^3), and it is also affected by the size of the throat (100 μm). The time needed to reach the maximum density may be reduced using smaller reservoirs. The dimension of the reservoir and throat also affect the time needed to completely evacuate the gas once the solenoid valve is closed. In this work, mechanical constraints related to the solenoid valve did not allow reducing the reservoir size. The maximum of the density of the diatomic hydrogen gas jet is reached after 70 ms with a valve opening duration of 40 ms [Fig. 5(a)]. Stabilization of a diatomic nitrogen gas flow takes 150 ms for an opening duration of 100 ms [Fig. 5(b)].

V. ION ACCELERATION WITH GAS JET

The gas jet target was tested at the PICO2000 facility at LULI. The laser delivers an average energy of about 50 J with a wavelength of 1053 nm and 1 ps pulse duration. The beam is focused into a 12 μm spot diameter (FWHM), which results in an intensity of about 5×10^{19} W/cm^2. We have employed the same Haskel booster and Clark-Cooper solenoid valve as in the test bench. Supersonic gas jet targets are produced, which could attain the critical density (n_c)

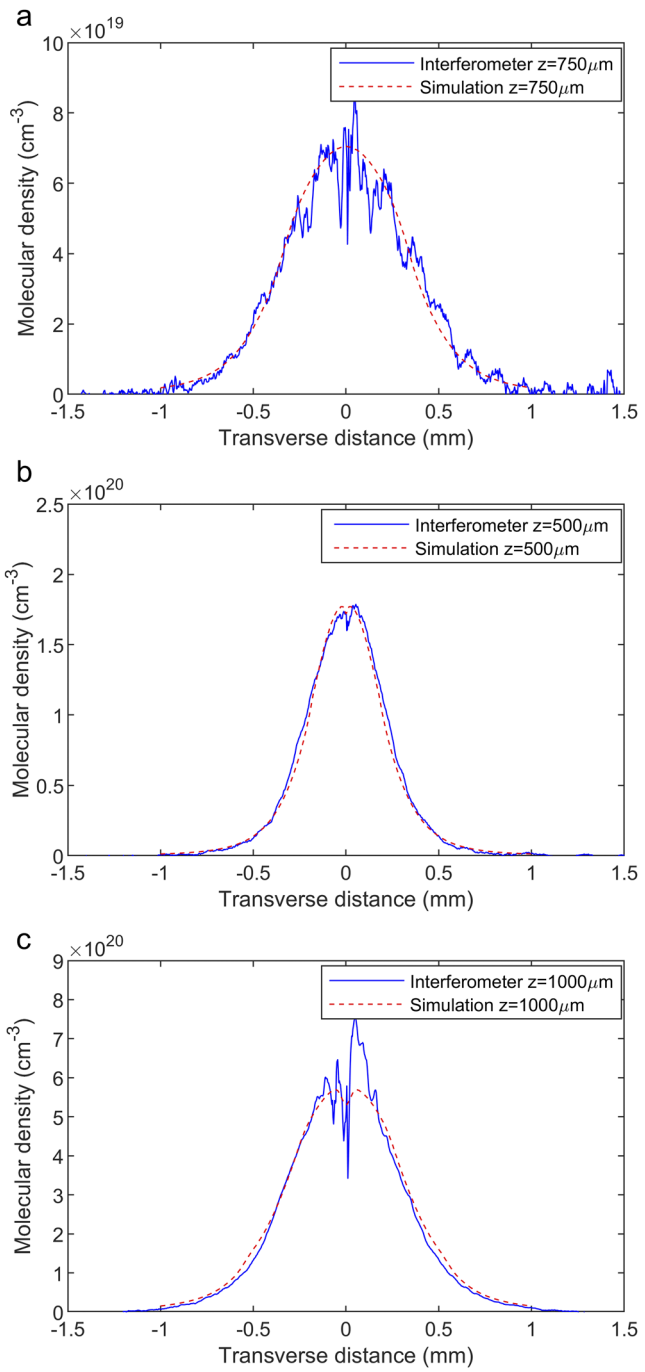

FIG. 4. Comparison of simulation results with interferometry reconstructions for (a) 100 bars diatomic hydrogen at Z = 750 μm, (b) 100 bars diatomic nitrogen at Z = 500 μm, and (c) 1000 bars diatomic nitrogen at Z = 1000 μm.

for the laser light radiation. Diatomic hydrogen is used as a target. The laser beam is focused at distances of 200 and 400 μm from the exit of the nozzle and at distances from the gas jet symmetry axis of −50 μm and −100 μm along the transverse direction, respectively

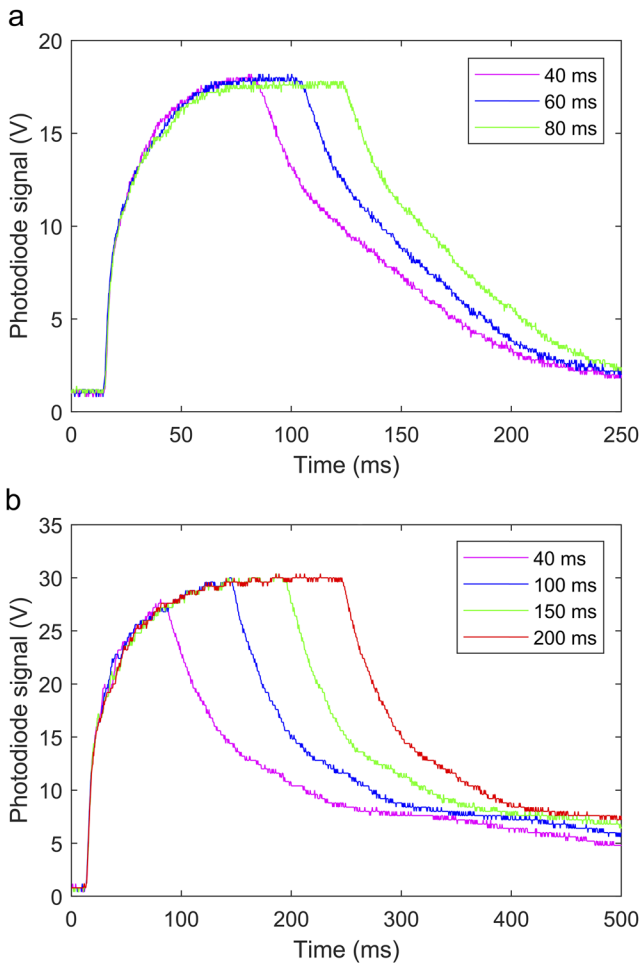

FIG. 5. Gas flow evolution of (a) diatomic hydrogen and (b) diatomic nitrogen gas jets as a function of time for different solenoid valve opening durations. The opening duration of the solenoid valve (triggered at t = 0 ms) is about 12 ms. After its closing, it takes several hundreds of milliseconds to empty the nozzle reservoir. The maximum density of the gas jet is reached in the plateau region.

(see Fig. 2). Four Thomson Parabola (TP) spectrometers are installed at 0°, 30°, 60°, and 90° with respect to the laser beam propagation to characterize the ionic emission (Fig. 6). A TP consists of a magnetic dipole followed by a pair of electric plates which allow us to measure the energy distributions of different ion species. BAS-TR imaging plates (IP) are used as sensitive detectors to record the particles.[31] TPs were calibrated measuring the magnetic field between the plates and then calculating the trajectories using GEANT4[32] and SIMION.[33] An example of the proton trace recorded on an imaging plate with a gas jet composed of diatomic hydrogen is shown in Fig. 7.

Figure 8 shows typical energy spectra of the protons detected by different TPs. A good shot-to-shot reproducibility is achieved. Best results (i.e., highest cut-off energies) were obtained at 200 μm from the nozzle exit. Up to 10^{13} protons/MeV/sr are detected following a continuous distribution up to 2 MeV. All TP spectrometers

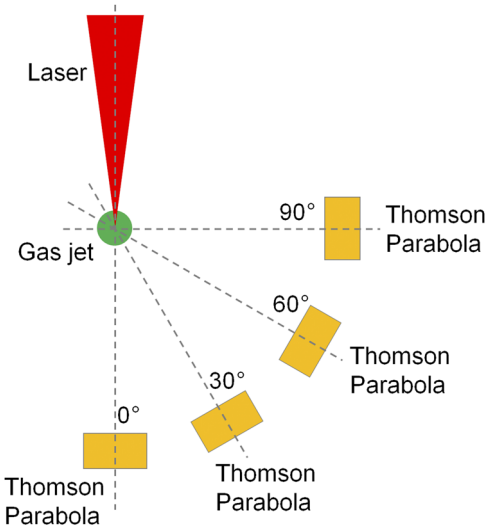

FIG. 6. Experimental setup at LULI with the configuration of four Thomson Parabolas at 0°, 30°, 60°, and 90°.

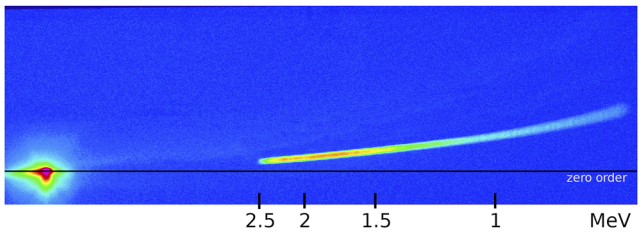

FIG. 7. Scan of the imaging plate showing the proton parabola recorded on the TP spectrometer placed at 0°. The red spot is due to the X-rays and UV light passing through the TP pinhole.

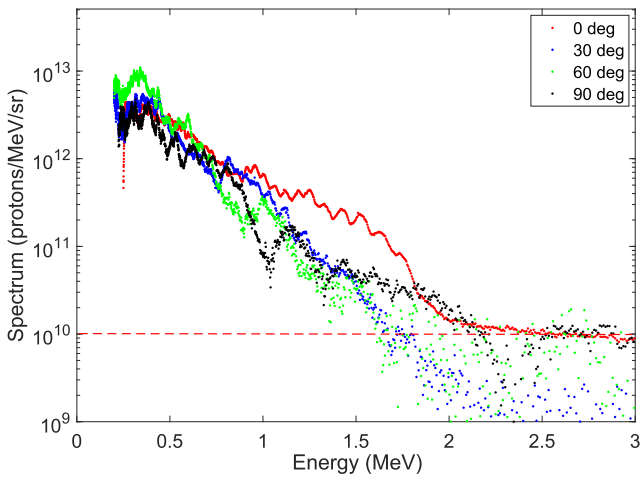

FIG. 8. Energy distribution of the protons detected at 0°, 30°, 60°, and 90° using a critical density diatomic hydrogen gas jet. The proton energy distribution is continuous up to 2 MeV. The experimental detection limit at 0° and 90° is 10^{10} protons/MeV/sr, and the detection limit at the other angles is a few 10^{9} protons/MeV/sr.

recorded nearly similar structures. A mechanism that could explain such an observation is ponderomotive laser channeling probably followed by laser collapse already reported by Ref. 14 in a near-critical plasma. This could push the electrons radially, and the ions are emitted in all directions. One should note that during the laser shot, the expanding plasma and the emitted particles strongly interact with the nozzle seriously damaging it, thus changing the properties of the gas jet target.

VI. CONCLUSION

A close to critical density supersonic gas jet target has been developed for laser-driven proton acceleration. In a first experiment, 10^{13} protons/MeV/sr with continuous energy distributions up to 2 MeV have been accelerated in the interaction with a 5×10^{19} W/cm^2 intensity laser. Thus, this experiment has proven ion acceleration using this nozzle. Particle-In-Cell (PIC) simulations are being performed to understand precisely the underlying acceleration mechanisms. The influence of the laser parameters on the ion energy distribution remains to be studied. Further development is ongoing to design nozzles capable of delivering similar density profiles further away from their exit in order to reduce the damage.

ACKNOWLEDGMENTS

The authors would like to thank the staff of the LULI facility and CENBG technical departments for their technical assistance during the experiment. This work was supported by ANR-17-CE30-0026-02, POPRA, and IN2P3-CNRS 2016-2020 (ALP-IONS projects) grants. M.E. and J.J.S. acknowledge financial support from the Programme IdEx Bordeaux—LAPHIA (Grant No. ANR-10-IDEX-03-02).

REFERENCES

[1] H. Daido, M. Nishiuchi, and A. S. Pirozhkov, "Review of laser-driven ion sources and their applications," Rep. Prog. Phys. **75**, 056401 (2012).
[2] L. Pommarel, B. Vauzour, F. Mégnin-Chanet, E. Bayart, O. Delmas, F. Goudjil, C. Nauraye, V. Letellier, F. Pouzoulet, F. Schillaci, F. Romano, V. Scuderi, G. A. P. Cirrone, E. Deutsch, A. Flacco, and V. Malka, "Spectral and spatial shaping of a laser-produced ion beam for radiation-biology experiments," Phys. Rev. Accel. Beams **20**, 032801 (2017).
[3] A. Macchi, M. Borghesi, and M. Passoni, "Ion acceleration by superintense laser-plasma interaction," Rev. Mod. Phys. **85**, 751–793 (2013) and references therein.
[4] M. Borghesi, "Laser-driven ion acceleration: State of the art and emerging mechanisms," Nucl. Instrum. Methods Phys. Res., Sect. A **740**, 6–9 (2014) and references therein.
[5] I. Prencipe, J. Fuchs, S. Pascarelli, D. W. Schumacher, R. B. Stephens, N. B. Alexander, R. Briggs, M. Büscher, M. O. Cernaianu, A. Choukourov *et al.*, "Targets for high repetition rate laser facilities: Needs, challenges and perspectives," High Power Laser Sci. Eng. **5**, e17 (2017).
[6] V. Malka, S. Fritzler, E. Lefebvre, M.-M. Aleonard, F. Burgy, J.-P. Chambaret, J.-F. Chemin, K. Krushelnick, G. Malka, S. P. D. Mangles, Z. Najmudin, M. Pittman, J.-P. Rousseau, J.-N. Scheurer, B. Walton, and A. E. Dangor, "Electron acceleration by a wake field forced by an intense ultrashort laser pulse," Science **298**, 1596–1600 (2002).
[7] J. Faure, Y. Glinec, A. Pukhov, S. Kiselev, S. Gordienko, E. Lefebvre, J.-P. Rousseau, F. Burgy, and V. Malka, "A laser–plasma accelerator producing monoenergetic electron beams," Nature **431**, 541–544 (2004).
[8] D. Guénot, D. Gustas, A. Vernier, B. Beaurepaire, F. Böhle, M. Bocoum, M. Lozano, A. Jullien, R. Lopez-Martens, A. Lifschitz, and J. Faure, "Relativistic electron beams driven by kHz single-cycle light pulses," Nat. Photonics **11**, 293 (2017).

[9]J. Faure, D. Gustas, D. Guénot, A. Vernier, F. Böhle, M. Ouillé, S. Haessler, R. Lopez-Martens, and A. Lifschitz, "A review of recent progress on laser-plasma acceleration at kHz repetition rate," Plasma Phys. Controlled Fusion **61**, 014012 (2018).
[10]O. Tresca, N. P. Dover, N. Cook, C. Maharjan, M. N. Polyanskiy, Z. Najmudin, P. Shkolnikov, and I. Pogorelsky, "Spectral modification of shock accelerated ions using a hydrodynamically shaped gas target," Phys. Rev. Lett. **115**, 094802 (2015).
[11]D. Haberberger, S. Tochitsky, F. Fiuza, C. Gong, R. A. Fonseca, L. O. Silva, W. B. Mori, and C. Joshi, "Collisionless shocks in laser-produced plasma generate monoenergetic high-energy proton beams," Nat. Phys. **8**, 95–99 (2012).
[12]C. A. J. Palmer, N. P. Dover, I. Pogorelsky, M. Babzien, G. I. Dudnikova, M. Ispiriyan, M. N. Polyanskiy, J. Schreiber, P. Shkolnikov, V. Yakimenko, and Z. Najmudin, "Monoenergetic proton beams accelerated by a radiation pressure driven shock," Phys. Rev. Lett. **106**, 014801 (2011).
[13]F. Sylla, M. Veltcheva, S. Kahaly, A. Flacco, and V. Malka, "Development and characterization of very dense submillimetric gas jets for laser-plasma interaction," Rev. Sci. Instrum. **83**, 033507 (2012).
[14]F. Sylla, A. Flacco, S. Kahaly, M. Veltcheva, A. Lifschitz, V. Malka, E. d'Humières, I. Andriyash, and V. Tikhonchuk, "Short intense laser pulse collapse in near-critical plasma," Phys. Rev. Lett. **110**, 085001 (2013).
[15]S. N. Chen, M. Vranic, T. Gangolf, E. Boella, P. Antici, M. Bailly-Grandvaux, P. Loiseau, H. Pépin, G. Revet, J. J. Santos, A. M. Schroer, M. Starodubtsev, O. Willi, L. O. Silva, E. d'Humières, and J. Fuchs, "Collimated protons accelerated from an overdense gas jet irradiated by a 1 μm wavelength high-intensity short-pulse laser," Sci. Rep. **7**, 2045–2322 (2017).
[16]E. d'Humières, A. Brantov, V. Yu. Bychenkov, and V. T. Tikhonchuk, "Optimization of laser-target interaction for proton acceleration," Phys. Plasmas **20**, 023103 (2013).
[17]M. Liu, S. M. Weng, Y. T. Li, D. W. Yuan, M. Chen, P. Mulser, Z. M. Sheng, M. Murakami, L. L. Yu, X. L. Zheng, and J. Zhang, "Collisionless electrostatic shock formation and ion acceleration in intense laser interactions with near critical density plasmas," Phys. Plasmas **23**, 113103 (2016).
[18]E. d'Humières, P. Antici, M. Glesser, J. Boeker, F. Cardelli, S. Chen, J. L. Feugeas, F. Filippi, M. Gauthier, A. Levy, P. Nicolaï, H. Pépin, L. Romagnani, M. Scisciò, V. T. Tikhonchuk, O. Willi, J. C. Kieffer, and J. Fuchs, "Investigation of laser ion acceleration in low-density targets using exploded foils," Plasma Phys. Controlled Fusion **55**, 124025 (2013).
[19]L. O. Silva, M. Marti, J. R. Davies, R. A. Fonseca, C. Ren, F. S. Tsung, and W. B. Mori, "Proton shock acceleration in laser-plasma interactions," Phys. Rev. Lett. **92**, 015002 (2004).
[20]ANSYS FLUENT Academic Research Mechanical, Release 18.1.
[21]K. Schmid and L. Veisz, "Supersonic gas jets for laser-plasma experiments," Rev. Sci. Instrum. **83**, 053304 (2012).
[22]J. L. Henares, T. Tarisien, P. Puyuelo, J.-R. Marquès, T. Nguyen-Bui, F. Gobet, X. Raymond, M. Versteegen, and F. Hannachi, "Optimization of critical-density gas jet targets for laser ion acceleration in the collisionless shockwave acceleration regime," J. Phys.: Conf. Ser. **1079**, 012004 (2018).
[23]NIST Reference Fluid Thermodynamic and Transport Properties Database (REFPROP), http://www.nist.gov/srd/nist23.htm, version 8.0.
[24]See http://www.peacesoftware.de for Peace software, Berndt Wischnewski, Richard-Wagner-Str. 49, 10585 Berlin.
[25]V. Malka, C. Coulaud, J. P. Geindre, V. Lopez, Z. Najmudin, D. Neely, and F. Amiranoff, "Characterization of neutral density profile in a wide range of pressure of cylindrical pulsed gas jets," Rev. Sci. Instrum. **71**, 2329–2333 (2000).
[26]See http://web.luli.polytechnique.fr/Neutrino/ for Neutrino, Alessandro Flacco and Tommaso Vinci.
[27]M. Born, E. Wolf, A. B. Bhatia, P. C. Clemmow, D. Gabor, A. R. Stokes, A. M. Taylor, P. A. Wayman, and W. L. Wilcock, *Principles of Optics: Electromagnetic Theory of Propagation, Interference and Diffraction of Light*, 7th ed. (Cambridge University Press, 1999).
[28]E. R. Peck and S. Huang, "Refractivity and dispersion of hydrogen in the visible and near infrared," J. Opt. Soc. Am. **67**, 1550–1554 (1977).
[29]J. A. Stone and A. Stejskal, "Using helium as a standard of refractive index: Correcting errors in a gas refractometer," Metrologia **41**, 189 (2004).
[30]A. Hirschberg, "Schlieren and shadowgraph techniques: Visualizing phenomena in transparent media: G.S. Settles (Springer-Verlag, Berlin, Germany, 2001)," Eur. J. Mech.: B/Fluids **21**, 493 (2002).
[31]T. Bonnet, M. Comet, D. Denis-Petit, F. Gobet, F. Hannachi, M. Tarisien, M. Versteegen, and M. M. Aleonard, "Response functions of Fuji imaging plates to monoenergetic protons in the energy range 0.6–3.2 mev," Rev. Sci. Instrum. **84**, 013508 (2013).
[32]S. Agostinelli *et al.*, "Geant4—A simulation toolkit," Nucl. Instrum. Methods Phys. Res., Sect. A **506**, 250–303 (2003).
[33]SIMION 3D v8.0/8.1, Scientific Instrument Services.